Highly-Efficient Peroxymonosulfate Activation for Sulfacetamide Degradation over Nitrogen-functionalized Graphene: The Effect of Thermal Annealing Temperature on Reactive Functional Groups

Xiao Chen, Teik-Thye Lim

School of Civil and Environmental Engineering, Nanyang Technological University, 50 Nanyang Avenue, Singapore 639798, Singapore
CTTLIM@ntu.edu.sg

Nitrogen-doped graphene (NG) prepared through thermal annealing of graphene oxide (GO) and urea was employed as a peroxymonosulfate (PMS) activator to degrade sulfacetamide (SAM). The fine tuning of the concentrations of functionalities and catalytic performance of NG was realized via tweaking thermal annealing temperature. NG600 (NG prepared at 600 °C) with the controlled N bonding configurations (a high N doping level (16.0 wt%) and a most optimum amount of pyridinic N (38.4 %N), pyrrolic N (31.8 %N), graphitic N (25.9 %N)) performed best as PMS activator. Quenching experiments disclosed that radical pathway contributed more to SAM degradation than non-radical pathway. $SO_4^{\cdot-}$ was the key reactive species for the SAM degradation in the NG/PMS system.

Key words: metal-free catalysis, nitrogen-doped graphene, peroxymonosulfate, sulfacetamide, sulfate radical

1. Introduction

Sulfonamides have a widespread distribution in the aquatic environment and induce the evolution of antibiotic resistant pathogenic bacteria, posing a threat to the ecosystem and human health even at a low concentration (Rizzo, Manaia et al. 2013). Sulfate radical-based advanced oxidation process (SR-AOP) which is based on sulfate radical ($SO_4^{\cdot-}$) is more effective to degrade persistent organic pollutants than conventional treatment process (e.g., filtration, flocculation or biological treatment) and traditional AOPs involving hydroxyl radical (HO$^{\cdot}$) (e.g., UV/H_2O_2, O_3/H_2O_2 or Fenton) due to the higher redox potential of $SO_4^{\cdot-}$ (E^o = 2.5-3.1 V) and its high half-life relative to its selectivity (30-40 μs), wide range of pH tolerance and slow utilization of precursor oxidants (Li, Wan et al. 2016). $SO_4^{\cdot-}$ as a strong oxidant can be produced by activation of peroxymonosulfate (PMS) or persulfate (PS) via scission of the peroxide O-O bond.

Nitrogen-doped graphene (NG) as a metal-free carbon-based catalyst can activate PMS to enhance the degradation performance of recalcitrant organics without toxic transition metal leaching from metal-activated PMS process (e.g., Co^{2+}/PMS), constant external energy supply for energy-based PMS activation process (e.g., UV/PMS, ultrasound/PMS or heat/PMS) and difficulty in separating and recovering homogeneous metal catalysts. Thermal annealing temperature plays a crucial role in the N doping content and N bonding configuration (Bai, Shi et al. 2016). Urea has been reported to be a superior nitrogen source over melamine and ammonium nitrate (Li, Duan et al. 2017). Previous studies about NG synthesized from urea under different synthesis temperatures involve applications other than environmental remediation, such as oxygen reduction reaction (Lin, Waller et al. 2012) or just investigation of the electrical properties of NG (Li, Yu et al. 2012). To the best of our knowledge, little information has been found about the effect of synthesis temperature on the catalytic performance of NG synthesized from urea as a nitrogen source for sulfacetamide (SAM) degradation via PMS activation. Herein, a comprehensive investigation of the effect of thermal annealing temperature (400, 500, 600, 700 and 800 °C) on the composition, structure and the synergistic SAM

adsorption and catalytic performance of NG synthesized from urea as a nitrogen source for SAM degradation via PMS activation was carried out.

2. Experimental

2.1 NG Synthesis

Graphene oxide (GO) was prepared via the modified Hummers' method (Hummers Jr and Offeman 1958). Generally, NG was prepared by thermal annealing of the dried mixture of 200 mg GO and 1 g urea at 400, 500, 600, 700 and 800 °C in the tubular furnace (N_2, 30 min, 5 °C min^{-1}), respectively. The final products (washed by a large amount of water and absolute ethanol in sequence and then dried at 60 °C in a vacuum oven overnight) were denoted as NG400, NG500, NG600, NG700 and NG800, respectively. Reduced graphene oxide (RGO600) was produced by the same procedure but without adding urea and calcined at 600 °C in a N_2 atmosphere. All the chemicals were of analytical grade (AR) and used without further purification.

2.2 Characterization

The characterization was done by X-ray diffraction (XRD, Bruker D8 Advance), field emission scanning electron microscopy (FESEM, JEOL JSM-7600F) and transmission electron microscopy (TEM, JEOL JEM-2010), Quantachrome Autosorb-1 analyzer (77K) for specific surface area (SSA) and pore size distribution, Fourier transform infra-red spectra (FTIR, PerkinElmer GX FTIR system), X-ray photoelectron spectroscopy (XPS, Kratos Axis Supra spectrophotometer), a PerkinElmer Series II 2400 CHNS/O analyzer and a LabRAM ARAMIS Horiba Jobin Yvon instrument with a 532-nm wavelength laser for Raman spectra.

2.3 Adsorption and Catalysis Evaluation

The catalytic performance of NG via PMS activation was evaluated through SAM degradation. The reaction took place in a 100-mL beaker with 50 mL SAM solution (10 mg L^{-1}), catalyst loading (0.2 g L^{-1}) and PMS dosage (0.5 mM PMS, which is commercially available in Oxone) and initial pH was adjusted to 7 with 1M NaOH. 0.5 mL of the aliquot was withdrawn at the designated time intervals and filtered through 0.45 μm membrane and injected into a vial, followed by adding 0.5 mL methanol as a quenching agent. Then the SAM concentration was measured by high-performance liquid chromatography (HPLC, PerkinElmer) (methanol: water = 6: 4, 0.6 mL min^{-1}, isocratic, UV λ_{max} = 256 nm). Reverse phase column (Hypersil Gold, 150 mm × 4.6 mm × 5 μm) was employed. The adsorption experiment was conducted following the same procedure without adding PMS. Phenol, sodium perchlorate ($NaClO_4$) and nitrobenzene (NB) were selected as quenching agents to investigate the possible catalytic mechanism in the NG/PMS system.

3. Results and Discussion

3.1 Characteristics of NG

As shown in FESEM images of Figure 1(a) - (c), the folding and exfoliation level of RGO600 was increased compared to GO with a smooth, wave-like structure. By contrast, NG was found to be more exfoliated, partially compacted and crumpled at the end of the doped graphitic sheets deriving from the defective sites caused by nitrogen doping. TEM images (Figure 1(d) - (f)) reveal that NG still maintained the characteristic two-dimensional planar structure of graphene after nitrogen doping, albeit with more wrinkles at the end of graphitic sheets. As shown in Figure 2(a). From NG400 to NG800, O/C ratio decreased as the annealing temperature increased, suggesting an enhancement of reduction level with increasing temperature due to more deoxygenation under higher annealing temperature. While a decreasing trend of N/C ratio was observed as the annealing temperature increased from 400 °C to 800 °C, owing to the scission of C-N bond under higher annealing temperature or the desorption of amine and amide from NG.
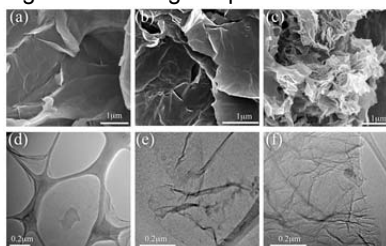

Figure 1: FESEM images of GO (a), RGO600 (b) and NG600 (c). TEM images of GO (d), RGO600 (e) and NG600 (f).
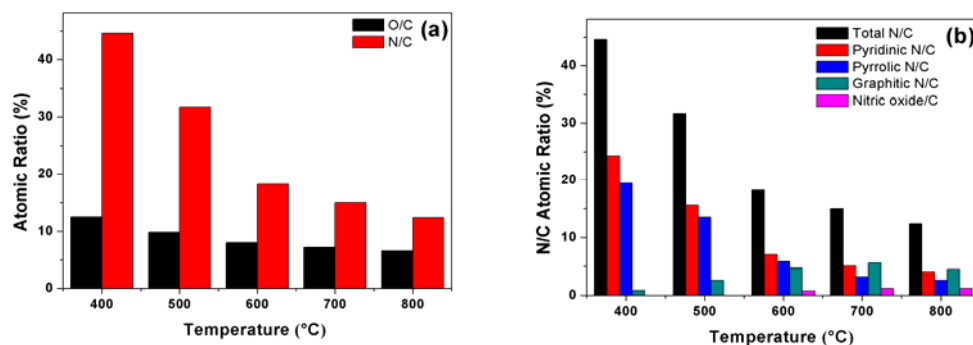
Figure 2: (a) Variation of nitrogen and oxygen contents in NGs with the annealing temperature. (b) Variation of total N, pyridinic N, pyrrolic N, graphitic N and nitric oxide contents with the annealing temperature.

According to XPS results in Figure 3 and Figure 2(b), N signals can be deconvoluted into pyridinic N (397.6 eV), pyrrolic N (399.2 eV), graphitic N (400.9 eV) and nitric oxide (N-O, 402.7 eV). NG600, NG700 and NG800 all had four types of nitrogen bonding configuration, NG400 and NG500 just possessed three types except for nitric oxide. More graphitic N was doped in the graphitic carbon network from 1.85 to 36.5 at.% as the annealing temperature increased from 400-800 °C and more nitric oxide (N-O) was incorporated into the graphitic platelets from 3.94 to 9.60 at.% as the annealing temperature increased from 600-800 °C due to the higher thermal stability of graphitic N and nitric oxide than pyrrolic N (Duan, Indrawirawan et al. 2015). The nitrogen doping level and compositional species can be adjusted by changing the thermal annealing temperature.
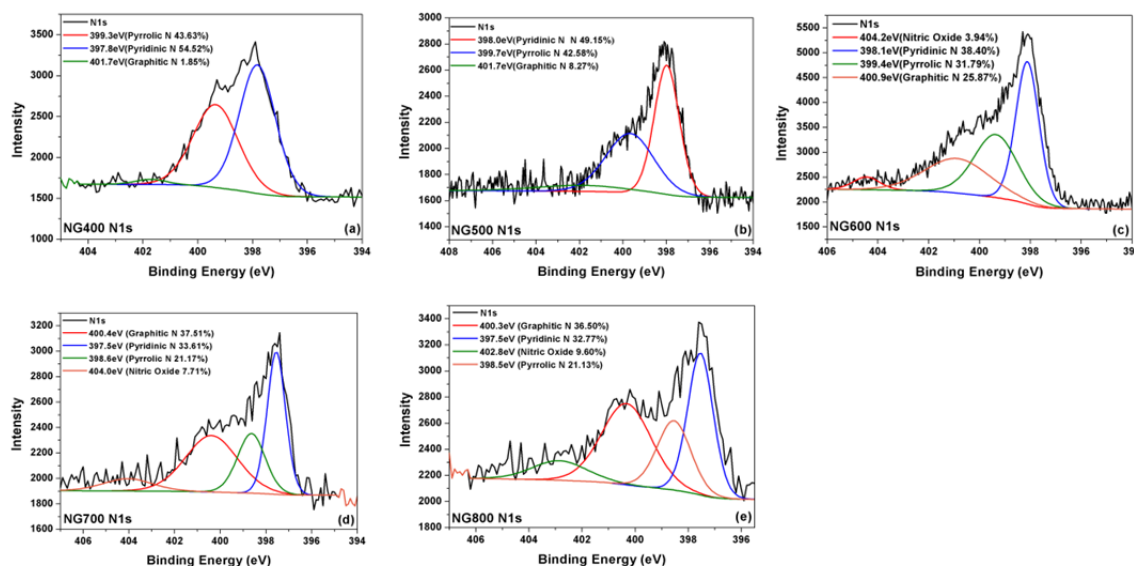

Figure 3: N1s scan of NG400 (a), NG500 (b), NG600 (c), NG700 (d) and NG800 (e).

XRD patterns of GO, RGO600 and NGs are shown in Figure 4(a), After nitrogen doping, the strong peak at $2\theta = 11°$ of GO disappeared in the XRD spectra of NGs and a new strong peak at around $2\theta = 26°$ emerged. It is interesting that NG400 still had a small peak at $2\theta = 11°$, which might be due to the inability of annealing temperature 400 °C to form well-structured NG (further explanation can be seen in the FTIR part, the tri-s-triazine unit was formed in NG400). The peaks of NGs at $2\theta = \sim42°$ all shifted to a higher 2θ degree and the peak intensity (the degree of the crystallinity) of NGs increased with the increasing annealing temperature, indicating better deoxygenation due to the elimination of oxygen functional groups and successful nitrogen doping.

As displayed in FTIR spectra of Figure 4(b), the intensities of C=O, C-O groups of NGs were reduced dramatically, indicating the intensive deoxygenation due to the removal of surface oxygen functional groups. The broad peak at 3413 cm^{-1} (vibration of O-H or water molecules) disappeared, suggesting an increment in

hydrophobicity of NG. C=C bond of NG shifted to a lower wavenumber (1553 cm^{-1}). A new peak at 1175 cm^{-1} emerged due to the formation of C-N bond and the residual C-O bond (Lin, Waller et al. 2012). Interestingly, a small peak at 785 cm^{-1} appeared at the FTIR spectrum of NG400 and NG500 (with lower intensity than that of NG400), which might be ascribed to the formation of tri-s-triazine (a type of nitrogen-containing heterocycle) (Costa and Camino 1988).

The ratio of I_D/I_G reveals the defective degree of carbon materials. As shown in Raman spectra of Figure 4(c), the I_D/I_G ratios of GO, RGO600, NG400, NG500, NG600, NG700 and NG800 are 0.906, 0.938, 1.099, 1.105, 1.115, 1.088 and 1.099, respectively. The increase in the ratio of I_D/I_G of NGs compared with that of GO and RGO600 indicates more defective sites after nitrogen doping, which is probably due to the introduction of nitrogen dopant, the creation of smaller-sized nanocrystalline graphitic domains and the loss of carbon atoms owing to the elimination of oxygen functional groups.
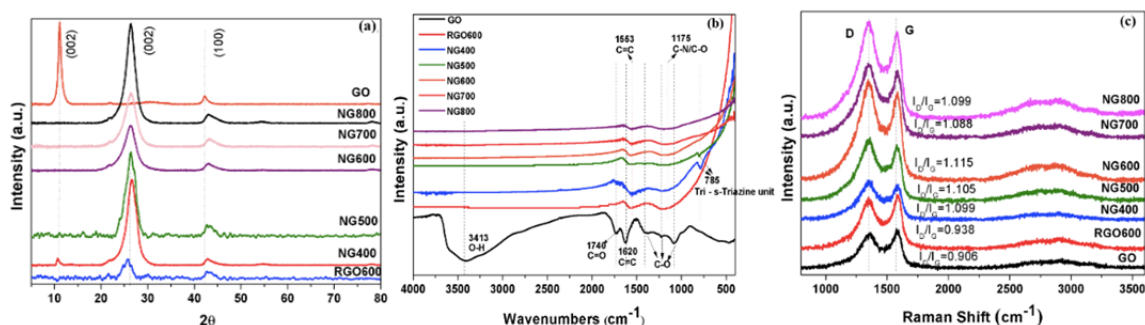

Figure 4: (a) XRD patterns, (b) FTIR spectra and (c) Raman spectra of GO, RGO and NGs.

The SSA, pore volume and pore size distribution of GO, RGO600 and NGs are shown in Table 1. The low SSA of GO (26 m^2 g^{-1}) was probably due to the severe stacking effect resulted from strong hydrogen bonding formed between oxygen functional groups on the GO layers. The highest SSA (452 m^2 g^{-1}) of RGO600 was due to deoxygenation and thermal expansion. The SSA and pore volume of NGs increased with the increasing thermal annealing temperature.

Table 1: SSA, pore volume and pore size information of GO, RGO and NGs.

Catalyst	BET SSA (m^2 g^{-1})	Average pore volume (cm^3 g^{-1})	Average pore size (nm)
GO	26	0.017	2.03
RGO600	452	0.441	2.02
NG400	25	0.060	2.03
NG500	24	0.056	2.03
NG600	74	0.164	2.02
NG700	131	0.238	2.01
NG800	140	0.243	2.03

3.2 Adsorption and Catalytic Performance of NG

As shown in Figure 5(a), less than 10% SAM adsorption was achieved by GO and NGs. RGO600 exhibited the highest adsorption ability with 34% SAM removal efficiency, probably due to its highest SSA (452 m^2 g^{-1}) (Table 1) and π-π stacking intraction between the more carbon-rich surface of RGO and the aromatic ring of SAM.

According to Figure 5(b), the apparent first order reaction rate constants (k_{app}) of SAM degradation via PMS activation by GO, RGO600, NG400-NG800 are estimated to be 0.0086, 0.019, 0.0081, 0.031, 0.090, 0.061 and 0.071 min^{-1}, respectively. Compared with the rate of SAM degradation by direct PMS oxidation (0.0095 min^{-1}), GO and NG400 can hardly activate PMS for SAM degradation with only 40% and 39% removal efficiency within 60 min, respectively. However, RGO600, NG500-NG800 all exhibited catalytic ability to activate PMS, and all the NG500-NG800 showed better catalytic performances than RGO600. The SAM degradation by NG600/PMS is 5 times and 10 times faster than that of RGO/PMS and GO/PMS, respectively, indicating the doped nitrogen under higher annealing temperature (600-800 °C) is the active site producing catalytic effect to activate PMS.
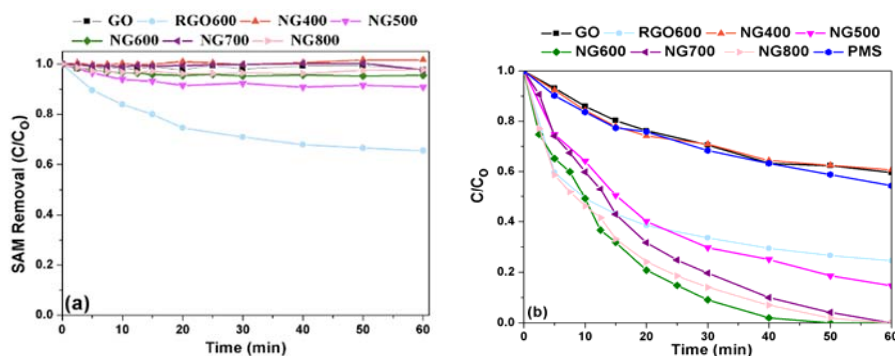
Figure 5: (a) adsorption performance and (b) catalytic performance of GO, RGO and NGs.

3.3 Mechanism of SAM Degradation by NG/PMS System

To investigate the possible SAM degradation mechanism in the present NG/PMS system, phenol was used to scavenge both $SO_4^{\cdot-}$ and $HO^\cdot$ with high and comparable rate constants (k ($SO_4^{\cdot-}$ + phenol) = 8.8×10^9 M^{-1} s^{-1}, k ($HO^\cdot$ + phenol) = 6.6×10^9 M^{-1} s^{-1}) (Lindsey and Tarr 2000, Ziajka and Pasiuk-Bronikowska 2005). $NaClO_4$ can contribute to the ionic strength of the NG/PMS system without inducing PMS activation and thus can act as a quenching agent for surface activated complex as non-radical pathway (Chen, Zhang et al. 2016). NB acted as a HO• scavenger (k (HO• + NB) = 3.9×10^9 M^{-1} s^{-1} > k ($SO_4^{\cdot-}$ + NB) (< 10^6 M^{-1} s^{-1})) (Neta, Madhavan et al. 1977, Buxton, Greenstock et al. 1988).
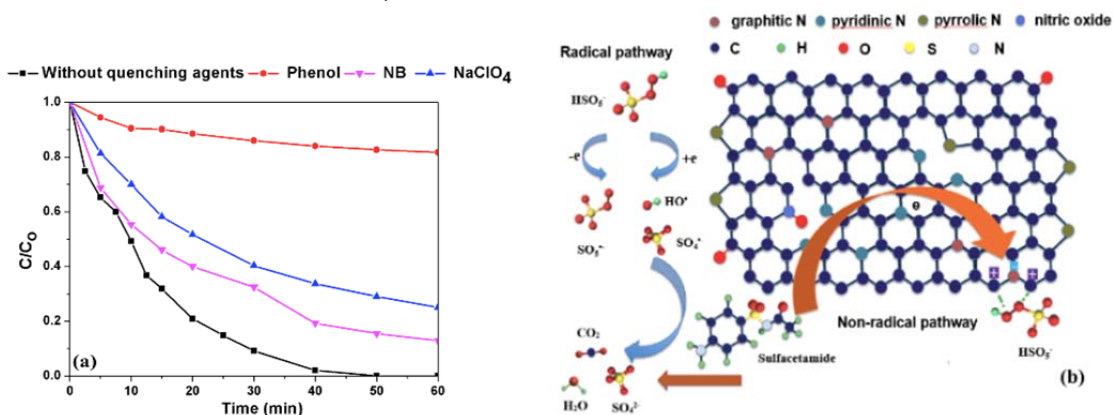

Figure 6: (a) The effect of phenol, $NaClO_4$ and NB as quenching agents on the SAM degradation by NG/PMS system (PMS = 0.5 mM, SAM concentration =10 mg L^{-1}, catalyst = 0.2 g L^{-1}, pH = 7, the mole ratio of phenol: SAM = 1000:1, NB = 25 mg L^{-1}, $NaClO_4$ = 0.8 M). (b) Mechanism of PMS activation and SAM degradation on NG.

As shown in Figure 6(a), only 18.3% SAM removal was achieved at a phenol/SAM molar ratio of 1000:1 within 60 min in the NG/PMS system. The addition of phenol hampered the SAM degradation much more significantly than that of NB or $NaClO_4$, indicating: 1) radical pathway (relative to pyridinic N and pyrrolic N) (Chen, Oh et al. 2018) contributed more to SAM degradation in the present NG/PMS system than non-radical pathway, which is also confirmed by the fact that NG600 possessed lower graphitic N level than NG700 and NG800 but demonstrated a better degradation performance; 2) between $SO4^{\cdot-}$ and HO•, the former is the key contributor to degrade SAM. The proposed mechanism of PMS activation and SAM degradation on NG is shown in Figure 6(b). Specifically, as for the radical pathway, the peroxide O-O bond in PMS was cleaved by the electrons transferred from the active sites of NG (e.g., defective sites, Lewis basic sites, etc.) to generate $SO_4^{\cdot-}$ and HO• to oxidize SAM. Regarding the non-radical pathway, the surface activated PMS was formed between the active site (comprising the negatively charged N atom and positively charged C atom due to the higher electronegativity of graphitic N than its adjacent C atoms) of NG and PMS via electrostatic bonding.

The reusability of NG600 was tested. The catalytic performance decreased from 100% SAM removal within 50 min of the 1st run to 92% SAM removal within 120 min of the 2nd run to 58% SAM removal within 120 min of the 3rd run. According to XPS analysis, the total N content of the NG600 remained unchanged (5% reduction

after 3rd run). However, the concentration of graphitic N (25.9 %N → 11.9 %N), pyridinic N (38.4 %N → 32.2 %N) and nitric oxide (3.94 %N → 3.34 %N) all decreased, whereas pyrrolic N increased from 31.8 %N to 52.2 %N, which indicates the change in the N bonding configuration accounts for the deactivation of NG600 besides the occupation of active sites by the adsorbed SAM intermediates. Further investigation can be put into developing more efficient and robust carbocatalysts with certain structures, such as the core-shell structure with excellent tunability and stability.

4. Conclusions

The high nitrogen doping levels (30.2-11.6 wt%) of NGs synthesized in this study manifested a negative correlation with annealing temperatures. The portion of graphitic N (1.85-36.5 at.%) and nitric oxide (3.94-9.60 at.%) correlated positively with the annealing temperature. NG endowed with catalytic activity should be synthesized under thermal annealing temperature of ≥ 500 °C. NG600 exhibited the best degradation performance via PMS activation for SAM decomposition due to N functionalities as active sites for PMS activation. Radical pathway with $SO_4^{\cdot-}$ as key factor contributed more to SAM degradation than non-radical pathway. This study offers an insight into the function of different surface N species to activate PMS, which promotes the advanced development in carbocatalysts design through chemical functionalization with the desired reactive species.

References

Bai, X., Y. Shi, J. Guo, L. Gao, K. Wang, Y. Du and T. Ma, 2016, Catalytic activities enhanced by abundant structural defects and balanced N distribution of N-doped graphene in oxygen reduction reaction, Journal of Power Sources, 306, 85-91.

Buxton, G. V., C. L. Greenstock, W. P. Helman and A. B. Ross, 1988, Critical Review of rate constants for reactions of hydrated electrons, hydrogen atoms and hydroxyl radicals ($\cdot$OH/$\cdot$O− in Aqueous Solution, Journal of Physical and Chemical Reference Data, 17(2), 513-886.

Chen, J., L. Zhang, T. Huang, W. Li, Y. Wang and Z. Wang, 2016, Decolorization of azo dye by peroxymonosulfate activated by carbon nanotube: Radical versus non-radical mechanism, Journal of Hazardous Materials, 320, 571-580.

Chen, X., W. D. Oh and T. T. Lim, 2018, Graphene- and CNTs-based carbocatalysts in persulfates activation: Material design and catalytic mechanisms, Chemical Engineering Journal, 354, 941-976.

Costa, L. and G. Camino, 1988, Thermal behaviour of melamine, Journal of Thermal Analysis, 34(2), 423-429.

Duan, X., S. Indrawirawan, H. Sun and S. Wang, 2015, Effects of nitrogen-, boron-, and phosphorus-doping or codoping on metal-free graphene catalysis, Catalysis Today, 249, 184-191.

Hummers Jr, W. S. and R. E. Offeman, 1958, Preparation of graphitic oxide, Journal of the American Chemical Society, 80(6), 1339.

Li, D., X. Duan, H. Sun, J. Kang, H. Zhang, M. O. Tade and S. Wang, 2017, Facile synthesis of nitrogen-doped graphene via low-temperature pyrolysis: The effects of precursors and annealing ambience on metal-free catalytic oxidation, Carbon, 115, 649-658.

Li, H., J. Wan, Y. Ma, Y. Wang, X. Chen and Z. Guan, 2016, Degradation of refractory dibutyl phthalate by peroxymonosulfate activated with novel catalysts cobalt metal-organic frameworks: Mechanism, performance, and stability, Journal of Hazardous Materials, 318, 154-163.

Li, X. J., X. X. Yu, J. Y. Liu, X. D. Fan, K. Zhang, H. B. Cai, N. Pan and X. P. Wang, 2012, Synthesis of nitrogen-doped graphene via thermal annealing graphene with urea, Chinese Journal of Chemical Physics, 25(3), 325-329.

Lin, Z., G. Waller, Y. Liu, M. Liu and C. P. Wong, 2012, Facile synthesis of nitrogen-doped graphene via pyrolysis of graphene oxide and urea, and its electrocatalytic activity toward the oxygen-reduction reaction, Advanced Energy Materials, 2(7), 884-888.

Lindsey, M. E. and M. A. Tarr, 2000, Inhibition of hydroxyl radical reaction with aromatics by dissolved natural organic matter, Environmental Science and Technology, 34(3), 444-449.

Neta, P., V. Madhavan, H. Zemel and R. W. Fessenden, 1977, Rate constants and mechanism of reaction of SO4•- with aromatic compounds, Journal of the American Chemical Society, 99(1), 163-164.

Rizzo, L., C. Manaia, C. Merlin, T. Schwartz, C. Dagot, M. C. Ploy, I. Michael and D. Fatta-Kassinos, 2013, Urban wastewater treatment plants as hotspots for antibiotic resistant bacteria and genes spread into the environment: A review, Science of the Total Environment, 447, 345-360.

Ziajka, J. and W. Pasiuk-Bronikowska, 2005, Rate constants for atmospheric trace organics scavenging SO4•- in the Fe-catalysed autoxidation of S(IV), Atmospheric Environment, 39(8), 1431-1438.